Fast Variable System Delay Correction for Spiral MRI

by

Payal Bhavsar

A Thesis Presented in Partial Fulfillment
of the Requirements for the Degree
Master of Science

Approved November 2013 by the
Graduate Supervisory Committee:

James Pipe, Co-Chair
David Frakes, Co-Chair
Vikram Kodibagkar

ARIZONA STATE UNIVERSITY

December 2013

ABSTRACT

Magnetic Resonance Imaging using spiral trajectories has many advantages in speed, efficiency in data-acquistion and robustness to motion and flow related artifacts. The increase in sampling speed, however, requires high performance of the gradient system. Hardware inaccuracies from system delays and eddy currents can cause spatial and temporal distortions in the encoding gradient waveforms. This causes sampling discrepancies between the actual and the ideal k-space trajectory. Reconstruction assuming an ideal trajectory can result in shading and blurring artifacts in spiral images.

Current methods to estimate such hardware errors require many modifications to the pulse sequence, phantom measurements or specialized hardware. This work presents a new method to estimate time-varying system delays for spiral-based trajectories. It requires a minor modification of a conventional stack-of-spirals sequence and analyzes data collected on three orthogonal cylinders. The method is fast, robust to off-resonance effects, requires no phantom measurements or specialized hardware and estimate variable system delays for the three gradient channels over the data-sampling period. The initial results are presented for acquired phantom and in-vivo data, which show a substantial reduction in the artifacts and improvement in the image quality.

ACKNOWLEDGEMENTS

First and foremost, I would like to thank my advisor, Dr. Jim Pipe for his dedicated support and mentorship. Thank you for always challenging me to come up with new ideas and for taking time to teach me many difficult concepts in MRI. Your immense knowledge and expertise has been invaluable in my graduate career.

Sincere, heartfelt thanks to my co-advisor Dr. Frakes, for your generous support, encouragement, and motivation in moving forward. Further, I would like to thank Dr. Kodibagkar for helpful discussions and guidance with my thesis.

I would also like to convey my deepest gratitude to my former mentors, Dr. Muthuswamy and Dr. Pizziconi. You have inspired me to pursue graduate school and your support has been imperative throughout my education.

Very special thanks to Haithem Babiker for being a true friend. Thank you for showing me the "double rainbow" when the times were hard!

I would also like to thank my colleagues at the Barrow Neurological Institute, BNI. Special thanks to Mike Schar for arranging the fun weekly hikes to Squaw Peak, Eric Aboussouan, for your encouragement, especially during ISMRM deadlines, Dinghui Wang, for your clear explanations of many complex topics in research and Chu-yu Lee, for the interesting discussions during the lunch breaks and advice on relationships. Many thanks to Nick Zwart, Ken Johnson, Ryan Robison, Ajit Devaraj, Dallas Turley, Sudarshan Ragunathan, Zhiqiang Li and Josef Debbins for your guidance with my research projects.

I would like to thank my parents and sister, to whom I am forever grateful for their patience and selfless love. Special thanks to Starbucks for providing me with free refills of coffee for the late nights at BNI. Lastly, I would like to acknowledge that this work was funded by GE Healthcare.

TABLE OF CONTENTS

LIST OF TABLES

LIST OF FIGURES

Chapter 1

INTRODUCTION

Magnetic Resonance Imaging (MRI) is a versatile, tomographic modality which offers superior contrast and sensitivity in soft-tissue imaging. It is a non-invasive, multiplanar technique which can provide high resolution images of the human body. MRI is used extensively in anatomical, functional, vascular and real-time imaging for diagnosis of many neural and cardiovascular diseases [25]. Due to its unique ability to achieve flexible contrast, it can be used to measure physical parameters such as diffusion, flow, temperature, chemical-shift and physiological processes such as functional activation and perfusion in the brain [23]. Compared to other imaging modalities like Computed Tomography (CT), Positron Emission Tomography (PET) and Single Photon Emission Computed Tomography (SPECT) which use ionizing radiation, MRI uses low energy radio-frequency (RF) waves and magnetic fields to create images of the biological tissue [40]. The image represents the spatial distribution of the magnetization of the resonant nuclei in the target volume.

The resonance signal is sampled at discrete time points and stored in spatial frequency space, also known as k-space. Conventionally, the data are sampled along a cartesian trajectory to fill a uniformly spaced grid in k-space. If sampled at Nyquist, the image can be reconstructed rapidly by applying an inverse Fourier transform [19]. Cartesian trajectories allow faster image reconstruction but can be slow and inefficient in data-acquisition. Longer scans affect not only the operational costs, but also the patient comfort during the exam. Much effort has been made in the recent years to design alternative "Non-Cartesian" trajectories to increase the speed and efficiency of a MRI exam.

Several Non-Cartesian trajectories have been proposed of which spiral has gained a lot of attention. Spiral trajectories have many advantages in speed, SNR efficiency, low gradient moments, robustness to motion and flow-related artifacts [14] [9]. They are also used in many dynamic applications to study cardiac motion, blood velocity, chemical-shift measurements, functional activation in brain and for faster acquisition of 3D volumetric data sets [14], [20]. Spiral scans require high gradient amplitudes and slew rates to reduce the data-acquisition period. The increase in sampling speed requires fast switching amplifiers and high accuracy of the gradient system. Hardware inaccuracies from system delays and eddy currents can cause spatial and temporal distortions in the desired gradient waveforms [3] . If not corrected, these errors can cause sampling discrepancies between the actual and the ideal k-space trajectory. Reconstruction assuming an ideal trajectory can result in ghosting, blurring, or shading artifacts in spiral images [9] [1].

Spiral sequences are more sensitive to hardware imperfections than conventional Cartesian scans. Modern scanners use active shielding and waveform pre-emphasis [2] to reduce the effects of long term eddy currents, primarily for conventional Cartesian scans. Any short term gradient errors that may remain and still cause severe distortions in spiral trajectories. Such errors are difficult to characterize since they can either be system dependent, sequence specific or could even be time-varying. Several methods have been proposed to characterize the MR gradient system or measure the actual k-space trajectory on the scanner [10]. Generally, such methods require phantom measurements, specialized hardware or many modifications to the pulse sequence.

This work presents a new method to estimate variable time-varying delays for spiral-based trajectories. The delays are measured along the sampling period for

the three gradient channels. The spiral k-space data are acquired and analyzed on three orthogonal overlapping cylinders. The method can be used a quick calibration run before the actual data collection. It can work with all gradients on, requires no phantom measurements, additional hardware, is immune to off-resonance effects, requires just a minor modification of the pulse sequence [7]. Further, it has been tested on simulated data and acquired data and validated using the method proposed by Alley et. al [2] and Robison et. al method [39].

The thesis will introduce the principles of MRI, spin dynamics, MR signal generation, localization and image formation. The basics of spiral imaging, image reconstruction and artifacts is discussed. This work addresses the problem of the accuracy of spatial encoding in spiral MRI. A new method is proposed to estimate time-varying system delays for spiral k-space trajectory. The thesis includes the theory, methods, results and analysis of the proposed method.

1.1 Background

MRI is based on the physical principles of Nuclear Magnetic Resonance (NMR) which were developed simultaneously by Bloch and Purcell in 1945 [29]. NMR, at the time, was used in spectroscopy to study the physical and chemical properties of organic compounds. The application of encoding the NMR signal using spatially varying gradients was found by Paul Lauterbur, who published the first NMR image in 1973 [24]. In the late 1970s, Peter Mansfield developed Echo Planar Imaging (EPI), a fast scanning technique to generate MR images within a few seconds. Since then, MRI has evolved continuously with advances in hardware, faster acquisition methods, new contrast mechanisms and enhanced reconstruction techniques.

This section gives a classical description of the physics of MRI and is followed by a discussion of spiral imaging and system delay correction.

1.2 Spin Dynamics

Nuclei of elements with an unpaired number of protons, electrons or neutrons have interesting properties in NMR. The subatomic particles contain a quantum mechanical property spin, which is intrinsic in nature [26]. Classically, the spin can be described as a particle rotating about its axis. A positively charged particle spinning about its axis induces a magnetic dipole moment μ. In addition to magnetism, the spinning charge also have mass which gives it an angular momentum J. The magnetic dipole moment is related to the angular momentum by the rate of precession or the Gyromagnetic ratio which is given by

$$\mu = \gamma\, J \tag{1.1}$$

where γ is Gyromagnetic ratio, measured in units of Hz/T and is specific for a given nucleus [8]. Among others, hydrogen nuclei are of most clinical relevance to MRI due to their natural abundance in the human body and sensitivity to magnetic field.
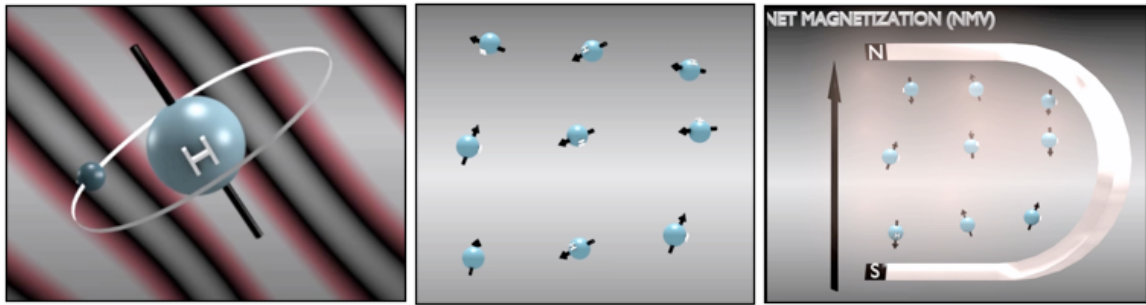
Figure 1.1: Magnetic dipole moment of hydrogen nuclei are randomly oriented in absence of a magnetic field. When an external magnetic field is applied, the nuclei have a preferred orientation relative to the applied field.

The nucleus of a hydrogen atom contains a single proton which exhibits a non-zero spin. In absence of an external magnetic field, the magnetic moments of the hydrogen nuclei are randomly oriented and have no preferred direction [29]. When placed in an external magnetic field B_0, the nuclei tend to align themselves relative to the direction of the applied field as shown in Fig.1.1. The B_0 exerts a torque to the magnetic moments changing the angular momentum, given by

$$\frac{dJ}{dt} = \mu \times B_0 \tag{1.2}$$

where B_0 is in units of Tesla (T). 1 Tesla is approximately 20,000 times stronger than the earth's magnetic field [38]. In hydrogen nuclei, two discrete energy states are

5

generated in the presence of B_0 due to Zeeman splitting [26]. The nuclei in the low energy state $N_\downarrow$ align parallel with the B_0 field while those in the high energy state $N_\uparrow$ align anti-parallel with the main field. The difference in the two energy states is given by Boltzmann distribution

$$\frac{N_\downarrow}{N_\uparrow} = e^{-\frac{\gamma \hbar B}{kT}} \tag{1.3}$$

where T is absolute temperature in Kelvin, $\hbar$ is the Planck's constant (1.05372 x 10^{-34} Joules seconds)and κ is the Boltzmann constant (1.38054 x 10^{-23} Joules/Kelvin) [30]. At room temperature, there are always more nuclei in the low energy state. The slight excess of the magnetic moments aligned in the parallel direction produce a net magnetization vector M. The B_0 field applies a torque to the spinning nuclei such that M gets"tipped" and precesses about the axis of the applied field. This is analogous to the precession of a spinning gyroscope in the influence of the earth's gravitational field. The rate of precession ω is measured in cycles/second can be calculated using

$$\omega = \gamma B_0 \tag{1.4}$$

The precessional frequency is known as the Larmor frequency and is directly proportional to the strength the B_0 field. In hydrogen nuclei, the γ is 42.57 MHz/T. Hence, at 1.5T, the Larmor frequency is approximately 64 MHz for a hydrogen proton.

The net magnetization can be divided into the transverse and the longitudinal components as shown in Fig.1.2. The transverse component M_{xy} represents the component of the magnetization which is perpendicular to B_0. The longitudinal component M_z is the component of the magnetization in the longitudinal direction with B_0.

6
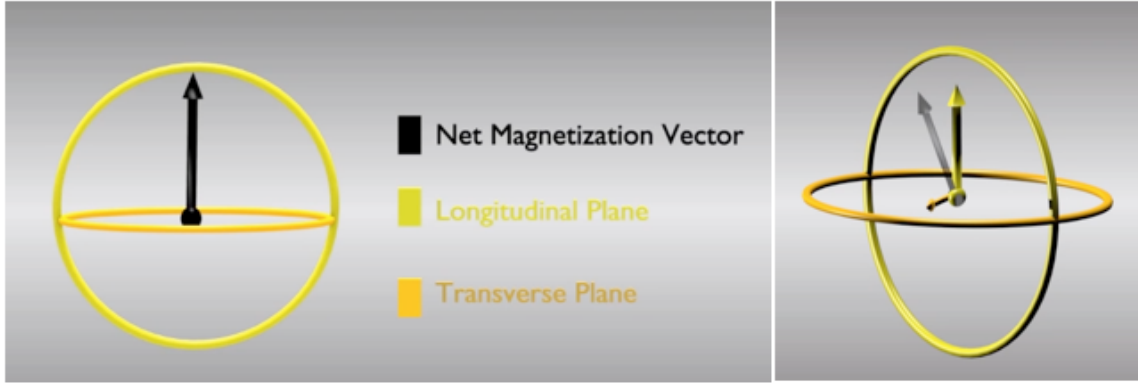
Figure 1.2: Net Magnetization vector has components in the longitudinal and the transverse plane and precesses about the total applied field.

$$M = M_{xy} + M_z \tag{1.5}$$

The magnetization is further manipulated using a radio frequency pulse (RF) tuned to the Larmor frequency of the precessing nuclei. The amplitude and duration of the RF pulse or B_1 determines the angle with which M gets tipped away from the z-axis to the transverse plane [38]. The flip angle α or the angle with which the net magnetization gets tipped is given by the

$$\alpha(\tau) = \gamma \int_0^\tau B_1(t)dt, \tag{1.6}$$

where τ is the duration of the RF pulse. The rotating magnetization in the transverse plane induces an electromagnetic force or voltage in the nearby receiver coils due to Faraday's law of induction. The signal is directly proportional to the number of resonant spins tipped in the transverse plane due to application of the RF pulse. The number of protons that contribute to the MR signal is a very small number, only 1 in 100,000 protons at 1.5T.

Once the RF pulse is turned off, the net magnetization returns to its equilibrium state through the process of relaxation [11]. As the nuclei return to their low energy state, the signal decays exponentially which is referred to as Free Induction Decay or FID. The time-dependent behavior of net magnetization M can be described by the Bloch equation.

$$\frac{dM}{dt} = \gamma M \times B - \frac{M_{xy}}{T_2} - \frac{M_z - M_z^0}{T_1} \tag{1.7}$$

The transverse component of the magnetization M_{xy} decays due to spin-spin interaction is given by the T_2 relaxation time. The net magnetization recovers in the longitudinal direction M_z back to its equilibrium state M_z^0 due to spin-lattice interaction is described by the time constant T_1. Both T_1 and T_2 relaxation times are characteristic of the tissue [26]. Different tissues have different T_1 and T_2 times depending on their physical and chemical properties. At 1.5T, the T_2 values of biological tissues is approximately in the range of 10-100 milliseconds and T_1 between 100-5000 milliseconds [30].

1.3 Spatial Encoding

The signal sampled in the coil is the total sum of the contribution of all the excited nuclei in the imaging volume. To localize the signal from different spins, spatial encoding is performed using magnetic field gradients as shown in Fig.1.3. The gradients change the total magnetic field as a function of position so that the precessional frequency of the spins are directly proportional o their position.

To select a slice, the RF and gradient are applied simultaneously to excite the spins in the region of interest. The excited magnetization has larmor frequencies
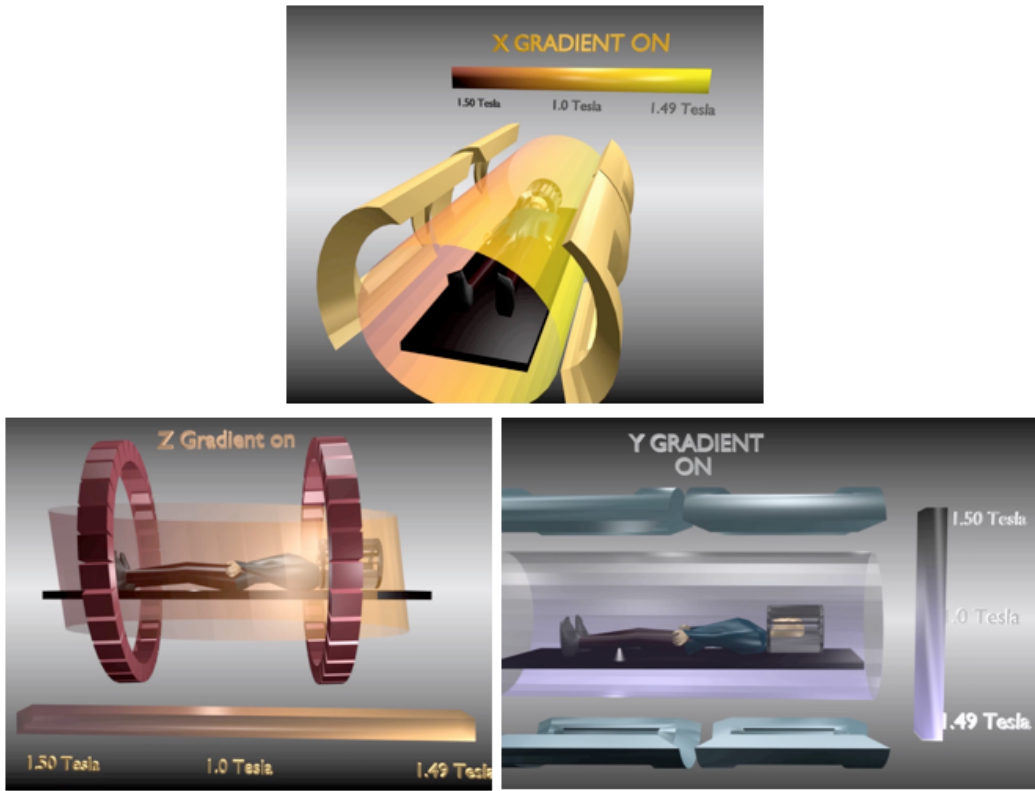
Figure 1.3: The three orthogonal gradients, X, Y and Z change the total magnetic field linearly in the applied direction.

within a certain bandwidth resonant with the applied band-limited RF pulse [30]. The location and the width of the slice can be carefully controlled by the gradient amplitude and the RF bandwidth as shown in as shown in Fig.1.4.

To acquire a slice thickness of Δz, the amplitude of the gradient G_z and RF bandwidth BW is calculated using

$$\Delta z = \frac{BW}{\gamma G_z} \qquad (1.8)$$
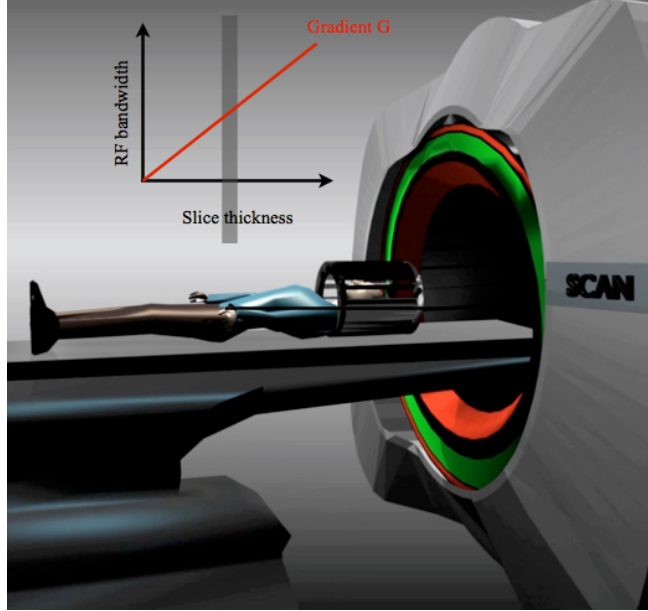
Figure 1.4: MRI uses a combination of RF and gradient fields to select a slice. Stronger gradients can be used to select a thin slice.

The gradient G_z causes a spatial variation in the frequencies and the precessing spins acquire a phase ϕ based on their position along z. The phase of a spin at a certain z position is the integral of the gradient and is given by

$$\Delta\phi(\vec{z}) = -\vec{z}[\gamma \int_0^t G_z(t)dt] \tag{1.9}$$

After slice selection, subsequent gradients perform phase and frequency encoding of the spins in the imaging slice. Spatial encoding can be applied in multiple directions to acquire 2D and 3D images of a given volume [8]. The time between each excitation pulse is known as repetition time (TR). The period between the RF pulse and the signal acquisition is the echo time (TE). The sequences are designed so that two parameters (TE and TR) can generate contrast between different tissue. The

resonant signal is acquired repeatedly using a sequence of RF pulses and gradient fields, also called a pulse sequence [29].

With developments in gradient hardware, there is also an increasing demand for faster pulse sequences. The standard Spoiled Gradient Recalled echo (SPGR) sequence uses smaller flip angles and stronger gradients to reduce both the TR and TE times of the acquisiton. It is mainly used to acquire T1 weighted MR images where the contrast is primarily dependent on the flip angle. The steady state condition for the SPGR sequence is given by

$$S = S_0 sin(\alpha) \frac{1 - e^{\frac{-T_R}{T_1}}}{1 - cos(\alpha)e^{\frac{-T_R}{T_1}}} e^{\frac{-t}{T_2^*}} \qquad (1.10)$$

where S_0 the equilibrium magnetization, and T_2^* is shorter than T_2 and represents the spin-spin relaxation time due to field inhomogeneities. The signal equation gives the relationship between the imaging parameters and the MR properties of the tissue to generate contrast in the images.

The acquired signal s(t) at a time t is the Fourier Transform of the transverse magnetization distribution given by m(x,y)

$$s(t) = \int_y \int_x m(x, y)e^{i[2\pi k_x(t)x + 2\pi k_y(t)y]}dxdy, \qquad (1.11)$$

where k_x(t) and k_y(t) are the spatial frequencies given by

$$k_x(t) = \frac{\gamma}{2\pi} \int_0^t G_x(\tau)d(\tau), \qquad (1.12)$$

11

$$k_y(t) = \frac{\gamma}{2\pi} \int_0^t G_y(\tau) d(\tau), \tag{1.13}$$

The data in k-space are collected at specific values k_x and k_y, or spatial frequencies of the object m(x,y). The fourier transform of the signal requires accurate knowledge of the k-space sampling locations $k_x(t)$ and $k_y(t)$. Any timing error in the gradient waveform can cause a discrepancy between the prescribed and the actual k-space sampling locations. Such gradient errors can be a results of time-varying system delays and eddy currents which can vary over the sampling period. For a given gradient axis with the time delay Δt, the resulting k-space trajectory is

$$\hat{k}(t) = \frac{\gamma}{2\pi} \int_0^t G(\tau - \Delta t) d(\tau) \tag{1.14}$$

The timing error in k-space is then $\Delta k = \hat{k}$(t) - k(t) = $\gamma G \Delta$t.

1.4 Fast Imaging

The MR signal is sampled at discrete time points along a trajectory S(k(t)) traced by the gradients G_x, G_y and G_z. The k-space trajectories are designed to reduce the scan time and reduce the number of sequence repetitions. Ideally, the trajectories to sample k-space uniformly, meet the Nyquist criterion and the hardware limitations.

Spiral trajectories offer an intrinsic advantage as they can cover k-space efficiently, and thereby, reducing the data-acquisition period. The trajectories are generally center-out and designed to trace an Archimedian spiral given by eq.1.15 [17].

$$k = A\theta e^{i\theta} \tag{1.15}$$

where k(t) = k_x(t) + ik_y(t) is the complex k-space vector and A = $\frac{N}{D}$, where N is the total number of interleaves and D is the FOV and θ is the azimuthal angle function of the spiral k-space trajectory.

The spiral radius is directly related to the angle in k-space as shown in Fig.1.5. In a single shot, the trajectory can acquire the strongest signal and highest spatial frequency at the center and at the maximum radius in k-space, respectively.

Spiral encoding methods use the gradients efficiently but are sensitive to the imperfections of the gradient hardware. Hardware limits of the maximum gradient amplitude and slew rate constrain the velocity and acceleration - design parameters of k-space trajectory. An important consideration in spiral acquisitions is the image reconstruction process since the k-space samples are acquired in a discrete, non-uniform spiral pattern.
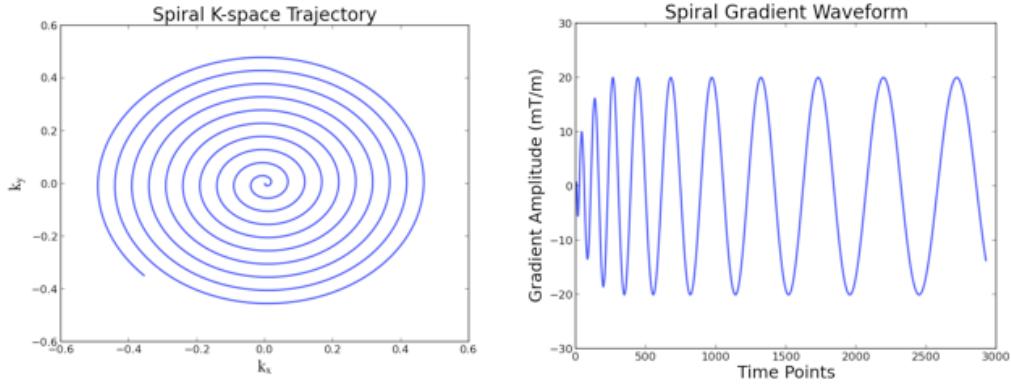
Figure 1.5: Spiral K-space trajectory and Gradient Waveform.

1.5 Image Reconstruction

The data in MR are acquired in k-space. The function f(x,y) represents the image, it Fourier Transform can be given by

$$m(x, y) = \int M(k_x, k_y) e^{i2\pi[k_x x + k_y y]} \tag{1.16}$$

For the spiral k-space data which lie on Non-Cartesian grid, cannot be inverted using a standard FFT to reconstruct the image. Gridding-based image reconstruction has been proposed to address this problem. The reconstruction is performed in three main steps, sampling density correction, convolution and inverse Fourier Transform. Common method used for sampling density correction are iterative, proposed by [36] and [37]. The data compensated for sampling density are convolved using a finite kernel and resampled onto a Cartesian grid. Once the data are space uniformly, the inverse FFT can be applied to reconstruct the image. The effect of convolving the data using a gridding kernel can be removed by applying a rolloff correction filter. This operation can be mathematically represented by

14

$$M_c = [(M \cdot S \cdot W) \otimes C] \cdot R \qquad (1.17)$$

where M_c is the gridded k-space data after the reconstruction process [21] . S are the series of discrete k-sampling locations, W is the weight applied for sample density correction and C is the gridding kernel to convolve the data and resample onto a uniformly spaced rectilinear grid R.

Gridding algorithms are designed to be computationally fast and free of reconstruction artifacts [5]. Optimization of the reconstruction process requires proper choice of the sample density function and the gridding kernel. The standard method used in image reconstruction of non-Cartesian data was developed by Jackson et. al [21] and the gridding process was optimized by Beatty et. al [5]. Inaccuracies in the reconstruction process can reduce the image quality and the Signal-to-Noise ratio (SNR). Accuracy of image reconstruction relies on precise knowledge of the actual sampling locations in k-space. The sampling locations in k-space can be altered due to system imperfections in the form of system delays and gradient amplitude distortions.

1.6 Gradient Imperfections

k-space sampling deviations can occur due to system delays, gradient amplifiers non-linearities, coil heating, switching delays, eddy currents or concomitant field gradients [1]. Gradient delay is a time delay between the actual and the prescribed start time of the gradient waveform. Another source is the timing error between gradient transmission and the data-acquisition [15]. Such timing errors can occur be due to poor system characterization, non-linearities of the system or poor eddy current

supression. The delays can change due to variation of the coil resistance with temperature [10]. Further, the delays in the three physical channels are independent of each other [13]. A system delay in spiral trajectories can cause more complex errors than a simple linear phase in case of Cartesian trajectories [1].

Fast pulsing magnetic fields produce transient eddy currents in the conducting system of the magnet and can substantially degrade the uniformity of the gradients. Precompensation is generally designed for a specific waveform for the MR system [28]. For spiral waveform, the gradient waveforms change continuously and therefore, the pre emphasis filters can sometime under or overcompensate the eddy currents induced deviations [10] .

1.7 State-of-the-Art

Modern scanners use active gradient shielding and waveform pre-emphasis, which mitigate, but do not completely eliminate the short-term gradient errors from system delays and eddy currents [10]. Several methods estimate these errors by measuring the actual k-space trajectory or characterizing the behavior of the gradient system. The k-space measurement techniques generally require phantom measurements, specialized hardware, or pulse sequence modifications.

The actual k-space trajectory can be measured directly using a so-called "self-encoding" method, originally proposed by Onodera et al. [31] and later extended by Takahashi and Peters [31] , Papadakis et al. [32] and Alley et al. [2]. This method can provide highly accurate results but requires many repetitions of the pulse sequence.

Other methods examine the signal-phase accrual due to multiple off-center excitations. Mason et al.'s approach [28] utilizes small test phantoms, placed at

16

different off-isocenter locations in the magnet system. The measurements can be acquired with a few repetitions of pulse sequence but requires precise knowledge of the test phantom locations. The slice-selection methods ([16], [41], [6]) are relatively simple, easy-to-implement and can be applied to any arbitrary test object. The accuracy of these methods, particularly for measurements at high spatial frequencies, depend mainly on the chosen slice thickness.

Recent methods use dedicated NMR probes [4], to measure the dynamic changes in magnetic fields. The probes can monitor the gradient fields in real-time and can provide a precise measurement of the actual k-space trajectory with each acquisition. These methods can be used directly on the test subject but requires specialized hardware.

Several methods estimate the k-space trajectory by characterizing the MR gradient system. Some of these model the behavior of the system delays ([18], [13], [34]) or eddy currents ([3], [27]), or directly use the system frequency response to correct different k-space trajectories used on the scanner ([1], [12]). These methods provide reasonable estimates assuming the gradient system errors are linear and time-invariant [10]. Robison et al. [39] estimates a single delay for each gradient channel using correlation-based estimates.

This work introduces a new method that extends Robison's approach by estimating continuous delays, with all gradients turned on. The measurements can be acquired for any spiral based trajectory with just a minor modification of the pulse sequence. The method includes gradient coupling effects, requires no phantom measurements and estimates the delays simultaneously for the three gradient channels over the data-sampling period [7].

17

1.8 Technique Description

The proposed method estimates time-varying system delays for stack-of-spirals based trajectories. It requires data-collection on three orthogonal cylinders, which overlap on the three orthogonal physical axes, as shown in Fig.1.6a. These delays occur in the direction of the trajectory, causing orthogonal shifts in the overlapping data at any given radius in k-space. In spiral trajectories, the radius increases monotonically as a function of the sampling period. The overlapping (orthogonal) data at any given radius correspond to the same time-of-acquisition and hence are affected similarly by off-resonance. These data are approximately the same, except for some noise effects and the shifts in the two orthogonal directions, which are estimated using a Fourier-based cross-correlation [7].

The estimated shifts are then decoupled and used to calculate the delay in the corresponding orthogonal gradients. Fig.1.6b illustrates a rectangular region of overlap and the corresponding data are seen in Fig.1.6c. The region of overlap for each plane was calculated at all radii of the trajectory, as shown in Fig.1.6d,e. For a given k-space radius k_r, the overlapping region on a plane is indicated by the blue shaded area (Fig.1.6d). The width x of this region is determined by the radius which allows a 50 percent overlap with the data of a given spiral interleaf shown by the gray shaded region. This width can be calculated by the following equation

$$x = \sqrt{k_r^2 - y^2}, \tag{1.18}$$

where y $= k_r$-d and d equals one half the total thickness of the plane, which gives

$$x = \sqrt{k_r^2 - (k_r - d)^2}, \tag{1.19}$$
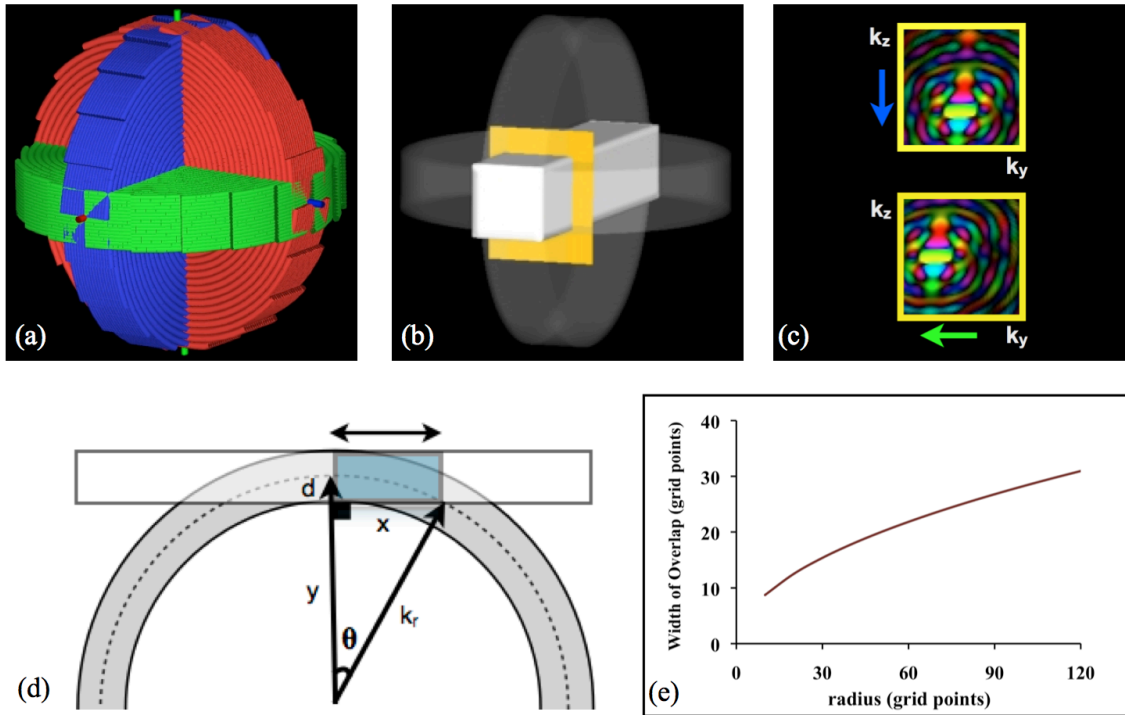
Figure 1.6: Orthogonal "stack-of-spirals" cylinders (a) are compared in (b) regions of overlap. The illustrated (yellow) plane in (b) has data from two cylinders (green and blue), each affected by delays from orthogonal gradients and hence shifted (c) in corresponding orthogonal directions (indicated by the green and blue arrows). For example, if this plane is normal to the X axis, the delays from the Y and Z gradients will shift the data (c) in the k_y and k_z directions, respectively. The color map in 1(c) indicates the signal phase of the k-space data. At a k-space radius of k_r, the width x illustrates the region of overlap shown by the blue shaded area in (d) for a given plane of thickness 2d. If θ is the angle between the radius and the vector normal to the plane of the overlap, then x can be determined by the radius at which there is a 50 overlap with the data of a spiral arm (shown in gray). For a grid matrix supporting a diameter of size 240, plot (e) shows the total width of the overlapping region (2*x) increases with radius in k-space.

For a grid supporting a matrix diameter of 240, equation [2] was used in the plot (Fig.1.6e) to calculate the total width of the overlapping region (2*x) versus the k-space radius. The plot shows the width of the overlap increases with the radius in k-space. The 2D correlation and subsequent delay estimation are described in the

Methods section. Similar pairs of overlapping data are compared at different radii of the trajectory for a continuous delay measurement through the sampling period.

Chapter 2

METHODS

This section describes the synthesis of data used for simulation, as well as experimental data collection. It then explains the data analysis and processing required for the proposed delay correction. The implementation of Alley's method [2] is also described for validation of experimental data.

2.1 Data Synthesis

System delays were simulated in the three gradient channels for a known k-space trajectory (described below in the Data Collection section). The delays were varied for each time-point of the sampling period, as shown in Fig.3.1. The altered (time-shifted) k-space coordinates were calculated using quadratic interpolation. Data were synthesized from a 3D image volume using the altered k-space trajectory. The proposed data analysis (discussed later) was then applied to estimate the delays for the altered trajectory set.

2.2 Data Collection

All experiments were performed on a 3.0T GE Signa Excite HDx system (General Electric, Milwaukee, WI), using an eight-channel head coil. Three cylindrical volumes (corresponding to Fig.1.6a), were collected from a GE phantom using a 3D SPGR stack-of-spirals sequence with relevant parameters FOV/res = 240/1mm, 64 interleaves, 24 planes, 10mm slice thickness, (TR/TE) of (20ms/4ms), flip angle of 20°, readout bandwidth of ± 250kHz, sampling period of 2.54ms and a total scan

time (for three cylinders) of 1.7 minutes. The experiment was repeated with 16 and 48 interleaves using the above parameters for a total sampling period of 9.53ms and 3.31ms, respectively. In-vivo data were also collected for 64 interleaves with the rest of the parameters kept the same.

2.3 Data Analysis

The following analysis was applied to both acquired and synthesized data sets in k-space. Data for each cylinder were corrected for sampling density [42] and gridded [5] on 3D Cartesian grid. The three Cartesian data sets were generated using an oversampling factor of 2 for the in-plane matrix. A roll-off correction was applied to the data in image-space, which were then cropped, and inverse Fourier transformed so that the final grid for each cylinder supported a 240 x 240 x 24 matrix in k-space. Planes corresponding to overlapping data on each grid were compared for shift estimation. The shift in the two orthogonal directions of overlapping data on each plane was estimated using a Fourier based cross-correlation.

2.4 Fourier-based Cross-Correlation

In a rectangular region of overlap (Fig.1.6b), system delay from a given cylinder comes from a single gradient and shifts the data in the direction of that gradient. If the plane is normal to the X axis, the delays from the Y and Z gradients will shift the overlapping data by Δk_y and Δk_z respectively. Let $f_1(k_y -\Delta k_y, k_z)$ and $f_2(k_y, k_z - \Delta k_z)$ correspond to the overlapping data from two orthogonal cylinders on the plane normal to the X axis as shown in Fig. 1c. The 2D correlation method in Ref. [22] was used to estimate these (translational) shifts in the k-space data

from the corresponding cylinders. The method is briefly explained here, and more implementation details can be found in Ref. [22]. These shifts in the two orthogonal directions were estimated from the location of the maximum correlation peak (p) of the functions f_1 and f_2, where

$$p = max|_{(\Delta k_y, \Delta k_z)}[\int f_1(k_y - \Delta k_y, k_z)f_2^*(k_y, k_z - \Delta k_z)dk_y dk_z] \qquad (2.1)$$

Using the Fourier shift property and Parseval's theorem,

$$p = max|_{(\Delta k_y, \Delta k_z)}[\int F_1(y, z)F_2^*(y, z)e^{-i(\Delta k_y y - \Delta k_z z)}dydz] \qquad (2.2)$$

where F_1 and F_2 are the Fourier Transforms of the functions f_1 and f_2 respectively, and * represents a complex conjugate. Equation [4] was used for the overlapping data on the other two spatial axes and the correlation peak was then used to estimate the k-space shifts for the respective data sets. For the planes normal to the Y and Z axes, the maximum peak was calculated for the shifts in (Δk_x, Δk_z) and (Δk_x, Δk_y), respectively.

2.5 System Delay Correction

For the proposed method, the system delay for a given axis is defined as the difference between the theoretical and the actual time when the integral of the gradient (i.e the k-space location) equals zero. Measurements are acquired for multiple spiral interleaves and at multiple zero-crossings to estimate the delay over the entire sampling period. At a given radius in k-space, the estimated shift (Δk) was used to calculate the system delay (Δt) using the approximation given in Ref. [39]

$$\frac{\Delta k}{\Delta t} = \gamma G sin\theta, \qquad\qquad (2.3)$$

where γ is the gyromagnetic ratio, G is the gradient amplitude and θ is the angle between the gradient and a vector describing the k-space location, shown in the inset of Fig.2.1b. If a plane is normal to the k-space vector, then the product $|G|sin\theta$ is the component of the gradient in this plane of the overlapping data, i.e in the angular direction. The measured shifts were used to calculate the delay in corresponding (orthogonal) gradient channels. Continuous delays were acquired by comparing overlapping planes along the entire length of each spatial axis. The correlation maps were averaged across data sets from eight coils prior to estimating the peak [max (p(Δk_y, Δk_z)] for each delay measurement.

At a given radius in k-space, a total of four delays were estimated for each gradient channel. For example, the delays for the X gradient were acquired by comparing overlapping planes normal to the +Y and -Y axes and +Z and -Z axes. The absolute delay for each physical gradient was calculated by averaging the estimates obtained on the four corresponding axes. The final averaged delays were used for each radius in k-space to correct the coordinates of the altered trajectory. The method was iterated by 1) re-gridding the data with the newly corrected trajectory, 2) using the same data-analysis and 3) estimating the residual delays. The delays for each of the three gradient channels were interpolated to obtain an estimate for each time-point of the sampling period.

The estimated delay was added to the k-space trajectory using polynomial interpolation. Let function k represent the uncorrected k-space coordinates, the new delay-corrected coordinates (i+Δ(i)) was generated using three neighboring sample

points k(i-1), k(i) and k(i+1), where i indicates the index of the sample and Δ is the delay added to each sample point. The new corrected k-space coordinate for a given time point t was calculated using the samples at the two endpoints a and b and the midpoint m = (a+b)/2, which gives the expression

$$k(t) = k(a)\frac{(t-m)(t-b)}{(a-m)(a-b)} + k(m)\frac{(t-a)(t-b)}{(m-a)(m-b)} + k(b)\frac{(t-a)(t-m)}{(b-a)(b-m)} \quad (2.4)$$

where t = (i+Δ(i))D, a =((i-1)D), m = ((i)D), b = ((i+1)D) and D is the sampling dwell time. Equation [6] was used to the estimate the delay-corrected k-space coordinates for each time point of the sampling period for the three gradient channels. To evaluate the effects of variable delays, a constant delay correction was applied using different constant delay values estimated by (i) averaging the constant part of the variable delays for each gradient channel (ii) using constants corresponding to the peaks of the variable delay curves and (iii) using the constant delays proposed by Robison et. al [22]. The method proposed by Robison et. al [39] was implemented on the same MR scanner as used for this work and the estimated delays in Ref. [22] were used here for sake of comparison. For acquired data, images were reconstructed without delay correction, using the first values of constant delays (i) and the (proposed) variable delay correction. Only the constant delays using (i) were used because they produced the image with the lowest root mean square (rms) error with respect to the reference image (discussed later as "Alley's method") compared to (ii) and (iii).

2.6 LSI model

The estimated delays for the proposed method are less reliable at the smaller radii in k-space as seen in Fig.2.1a (solid line). This is due to the radial nature of the trajectory as examined in Fig.2.1b, a plot of θ versus the data-sampling time. The trajectory starts out radially at $\theta = 0°$ and later becomes angular as θ approaches $90°$. This method analyzes the angular component of the trajectory and hence fails in the initial regions of k-space. To estimate the delays in these regions, a Linear-Shift Invariant (LSI) model was used, assuming that the system delays are a function of the gradient angular frequency, (the measured data are plotted in Fig.2.1d). For a given k-space radius k_r, the gradient angular frequency is defined as

$$\frac{d\alpha}{dt} = \frac{\gamma G sin\theta}{k_r},$$

(2.5)

where α is the angle of the gradient vector. The plot of the gradient angular frequency (Fig.2.1c) showed a single peak in the beginning of the frequency curve. The delays prior to the peak were calculated from the estimated delays corresponding to similar angular frequencies after this peak.

2.7 Validation with Alley's method

The method proposed by Alley [2] can provide an accurate measure of the actual k-space trajectory, estimating both system delays and eddy currents effects. The method was implemented (for acquired data only) both to estimate the "true" k-space trajectory as well as to independently estimate system delays (only). Note the same trajectory was used as described in the data-collection section. The k-space
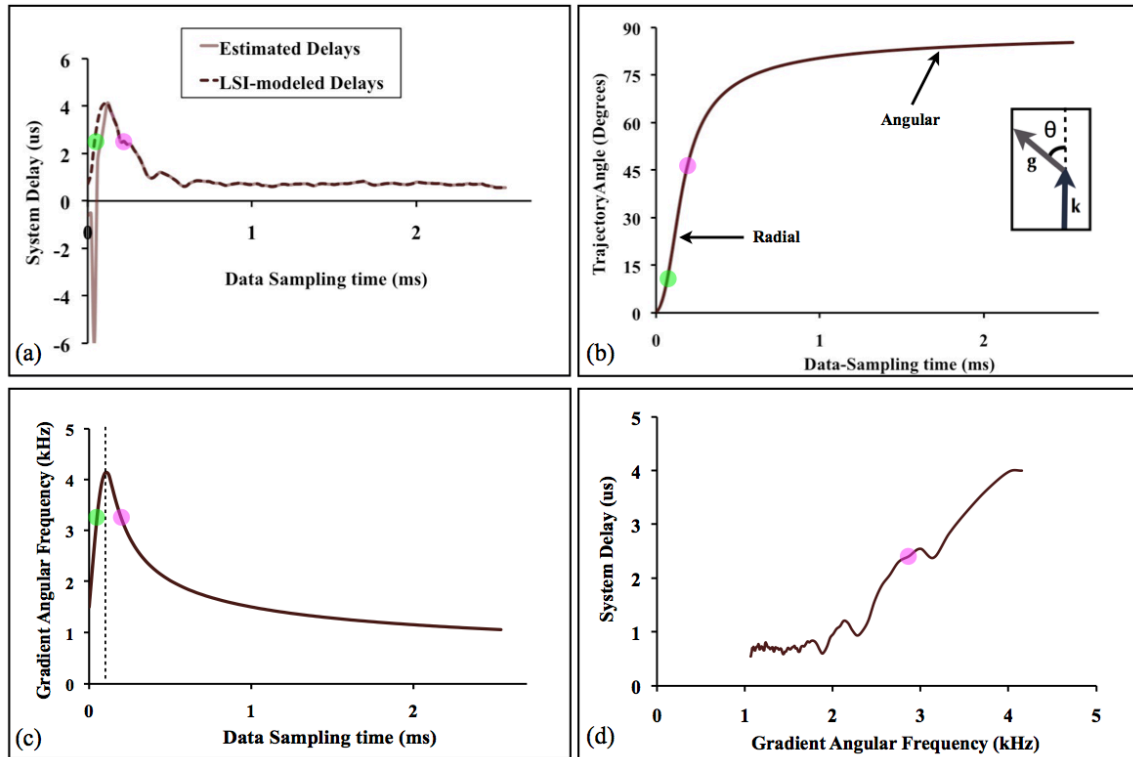
Figure 2.1: The uncorrected delays (a) estimated for a single gradient channel are less reliable in the more radial part of the trajectory (b), since this method measures the angular component of the delays in k-space. The gradient angular frequency (c) and an assumption that systematic delays are a function of that frequency (d) allows one to take measured delays to the right of the dotted line in (c) (i.e. magenta) and calculate a corresponding delay for times to the left of that dotted line (i.e. green). The final, corrected delays are shown (dashed line) in (a).

trajectory was measured separately for each spiral interleaf of the 64-interleaved set. To estimate the system delays, both the measured and the theoretical trajectory were plotted as a function of the data-sampling time [7].

The delays were measured at the zero-crossings in k-space (as illustrated in Fig.??), assuming the amplitude deviations are negligible in these regions. The delays for all 64 interleaves were combined to create a finely sampled delay estimate over the data-sampling time. The process was repeated for all three gradient channels.

27
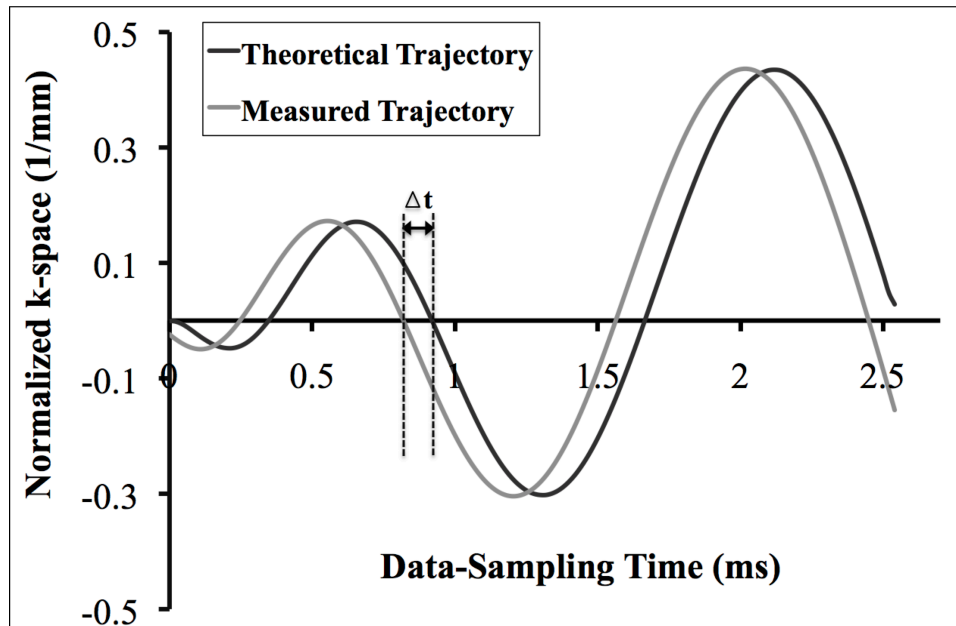
Figure 2.2: The delay (Δt) measured at the zero-crossing in k-space (exaggerated for clarity) by comparing the measured (using Alley's method) and the theoretical trajectory for each spiral interleaf.

Images were reconstructed using the fully measured k-space trajectory and using the measurements for system delays (only). The image reconstructed using the full measurement of the k-space trajectory was used as a reference image to analyze the performance of the proposed method. The total acquisition time for Alley's method was approximately 4 hours 48 minutes.

Chapter 3

RESULTS

3.1 Simulation

The estimated delays from the first and second iteration of the proposed method are
shown in Fig.3.1 are in close agreement with the simulated delays.
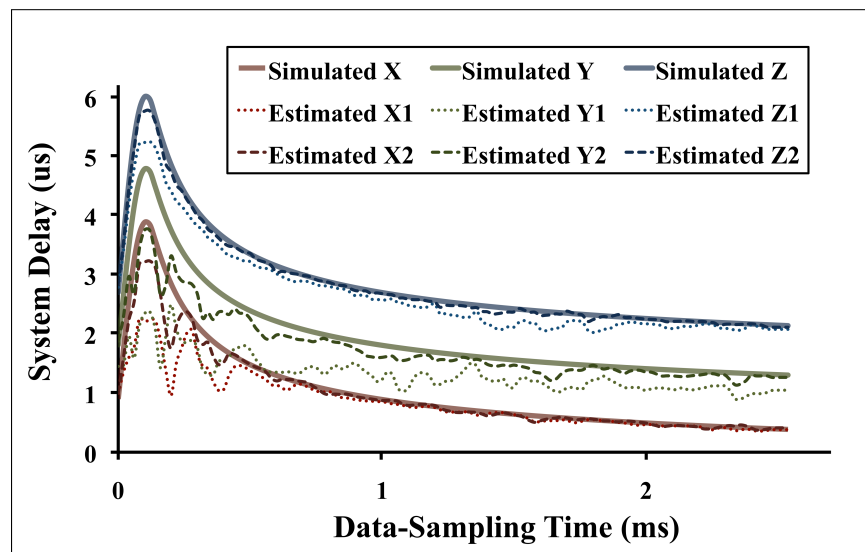
Figure 3.1: Variable system delays applied to synthesized stack-of-spirals data in
the three gradient channels. The estimated delays from the first (X_1, Y_1, and Z_1)
and second (X_2, Y_2 and Z_2) iterations illustrate the performance of the method in
estimating the applied delays. The results show that the second iteration improves
the accuracy of the estimates.

3.2 Experiments

The results of the two iterations of the proposed method are quite similar for 16,
48 and 64 interleaves as shown in Fig.3.2a-c respectively. Figure 3.3a-c shows the
dependence of the estimated delays to the gradient angular frequency for the X, Y

and Z gradients, respectively. The X gradient shows a greater frequency dependence compared to the Y and Z gradients. The method proposed was by Robison et. al [39] was implemented on the same MR system as used for this work. The estimated delays for the X and Y gradients shown in Fig.3.4 of (Ref. [39]) were also plotted here for sake of comparison, (Fig.3.3a,b). A $1\mu s$ delay was subtracted from Robison's estimates for the X and Y gradients to account for the differences in dwell times used between the two methods (i.e. $4\mu s$ in [39] versus $2\mu s$ used for the proposed method, respectively). For a dwell time of $2\mu s$ or $4\mu s$, the actual sampling starts at 1 or $2\mu s$, respectively, resulting in a $1\mu s$ discrepancy between the measured delays between the two methods. Figure 3.4 shows a good agreement between the estimated delays for the proposed method and those acquired for Alley's method [2]. The estimates are within $1\mu s$ of the reference delays, which in our experience do not result in visible changes in the reconstructed images [7].

Axial and coronal images for acquired data using a GE phantom are shown in Figures3.5 and 3.6 , respectively. The reconstruction using any of these delays showed a substantial reduction in artifacts (Fig.3.5 and Fig.3.6 c-e) compared to the uncorrected image (Fig. 3.5and Fig. 3.6a). Full use of the measured trajectory using Alley's method Fig. 3.5 and Fig. 3.6b showed slightly better artifact reduction than the sole use of delays. The apparent increased noise (speckle artifact) (Fig. 3.5 and Fig. 3.6b) may be a result of insufficient filtering of the k-space coordinates generated using the fully measured Alley's trajectory. The correction using single constant delays $0.75\mu s$, $2.23\mu s$ and $2.82\mu s$ for the X, Y and Z gradients, respectively, resulted in substantially more artifacts than when using a variable delay, (Fig. 3.5 and Fig. 3.6f).
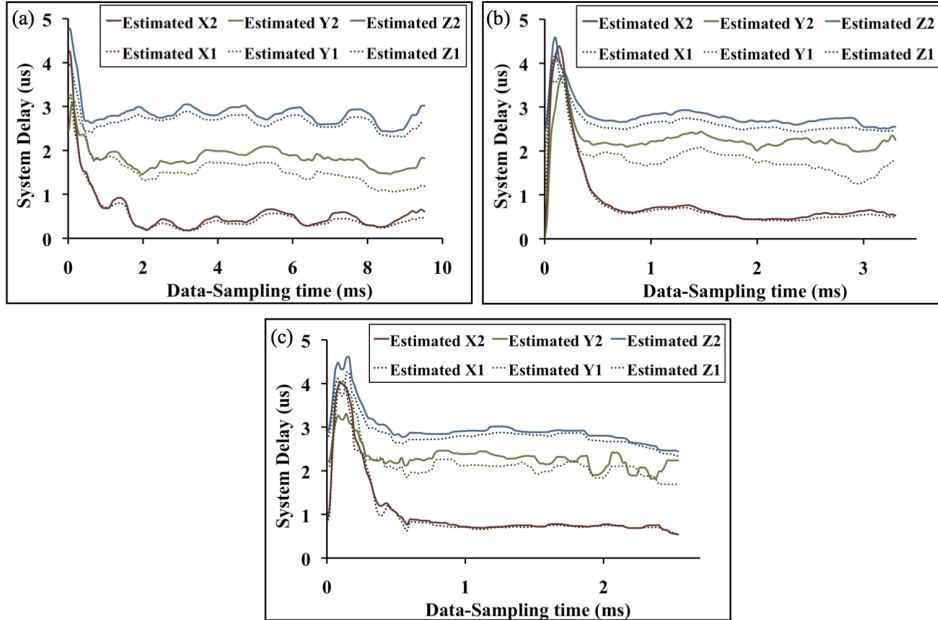
Figure 3.2: . The estimated delays using the first (X_1, Y_1, and Z_1)and second (X_2, Y_2, and Z_2) iteration of the proposed method are compared for a (a) 16, (b) 48 and (c) 64 interleaf trajectory. The results of the two iterations are quite similar.

Table 3.1: RMS error for Correction Methods

Proposed	Alley's	Constant	Robison's	Variable Peak
0.52	0.53	0.60	0.61	0.75

Assuming a maximum residual error of 1 for the uncorrected image (Fig. 3.5a), the relative root mean square error of the difference images (Fig. 3.5g-i) was 0.52, 0.53 and 0.60 respectively as shown in table3.1. For constant delays using Robison's estimates (X: 2μs and Y: 4μs) given in Ref. [39] and for those corresponding to peaks of the variable delay estimates (X: 4μs and Y: 3μs) shown in Fig. 3.2c, the relative root mean square error was 0.61 and 0.75, respectively. Figure 10 shows an example of using the correction on in-vivo data. The blurring artifacts in Fig. 3.7a were reduced greatly by using the proposed correction, (Fig. 3.7b). This method has also been tested on a 3D center out spiral-based trajectory "FLORET" [35] presented in Ref. [33].

31
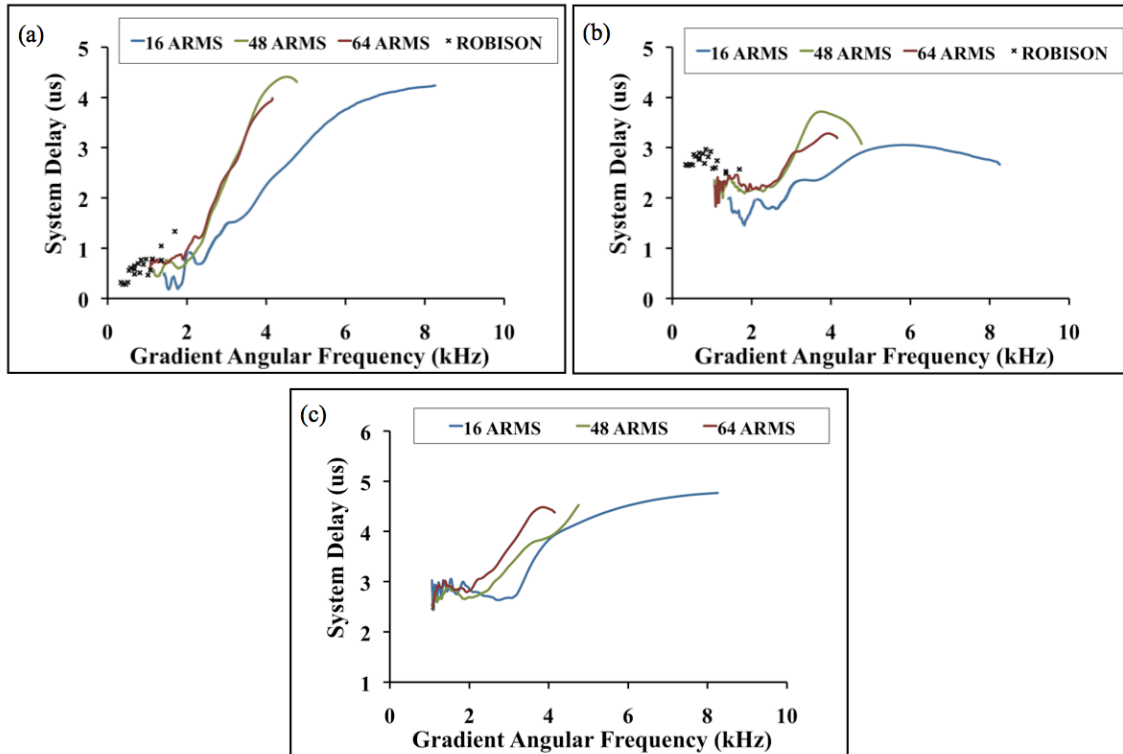
Figure 3.3: Estimated delays for the (a) X, (b) Y and (c) Z gradients are plotted for different number of interleaves (16, 48 and 64) as a function of the gradient angular frequency. The delay estimates shown in Fig. 7 of Ref 20 for the X and Y gradients are plotted for sake of validation. A delay of $1\mu s$ was subtracted from Robison et. al's [39] estimates in (a) and (b) to account for the discrepancy in the dwell times of $4\mu s$ and $2\mu s$ used in Ref. 20 and the proposed method, respectively.

32
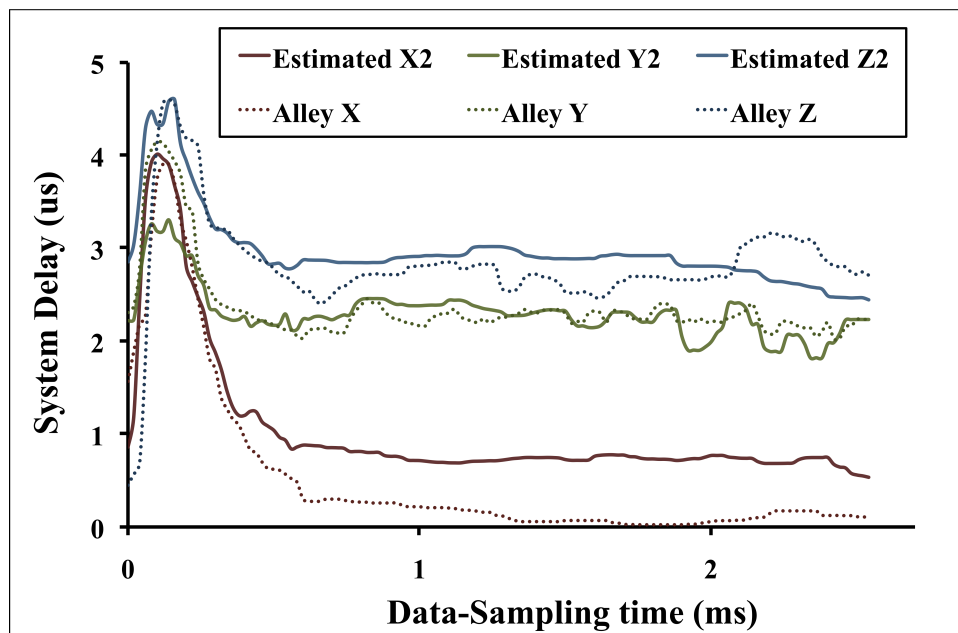
Figure 3.4: The estimated delays using a second iteration of the proposed method are compared to the delay measurements for Alley's method. The results for the three gradient channels are within 1μs of the reference delays.
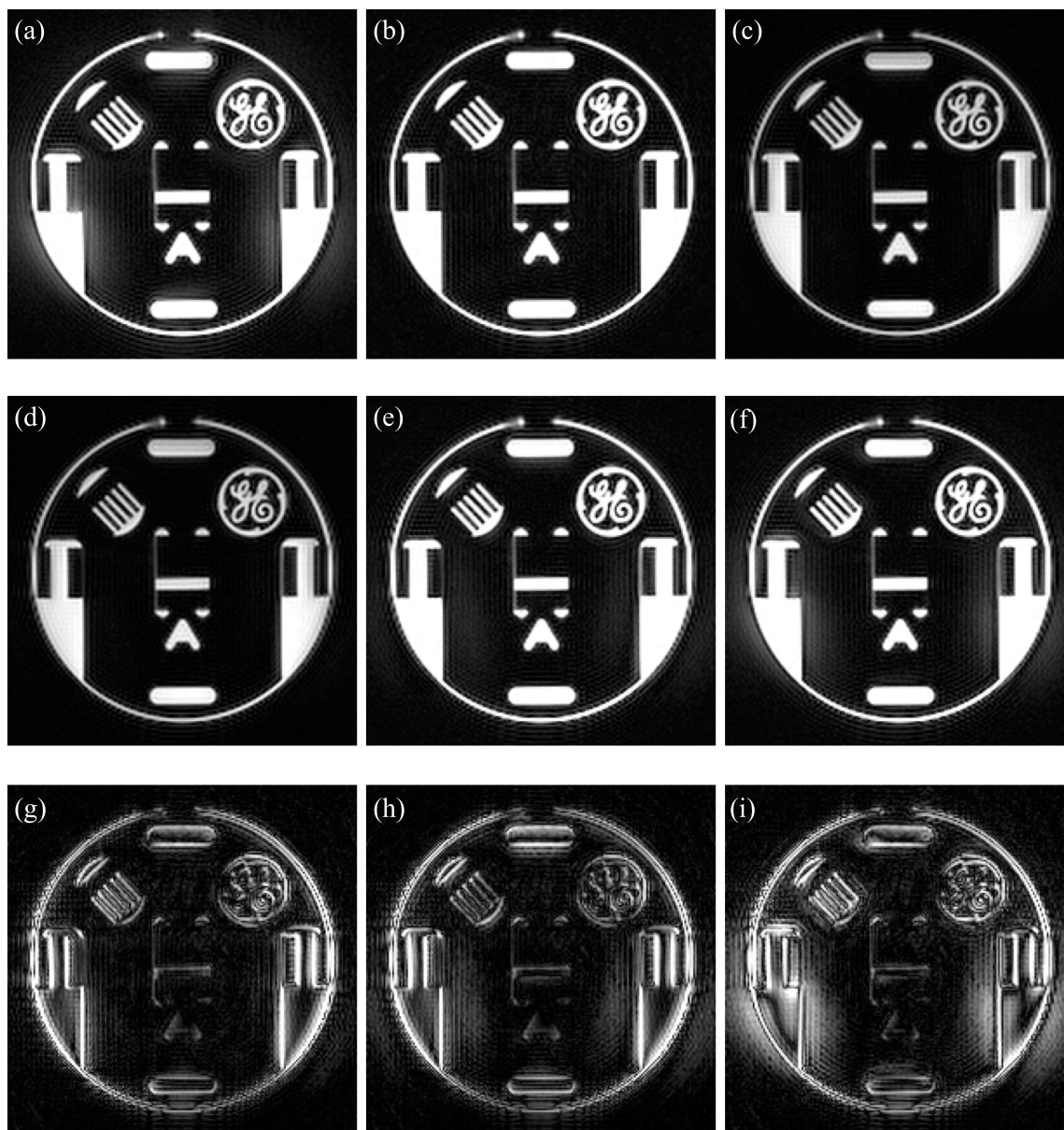
Figure 3.5: Axial images of acquired phantom data are reconstructed (a) with no correction, (b) with the full k-space trajectory measured using Alley's method, using delays estimated from the (c) first and (d) second iteration of the proposed method, (e) using delays measurements from Alley's method and (f) using constant delays for (X: $+0.75\mu s$, Y: $+2.23\mu s$ and Z: $+2.82\mu s$) gradients. The images in (g-i) represent the magnitude of the difference between the respective images in (d-f) and (b), which is assumed to be closest to the truth. The difference images (g-i) are scaled by a factor of 10 compared to the images (a-f) which are windowed the same.
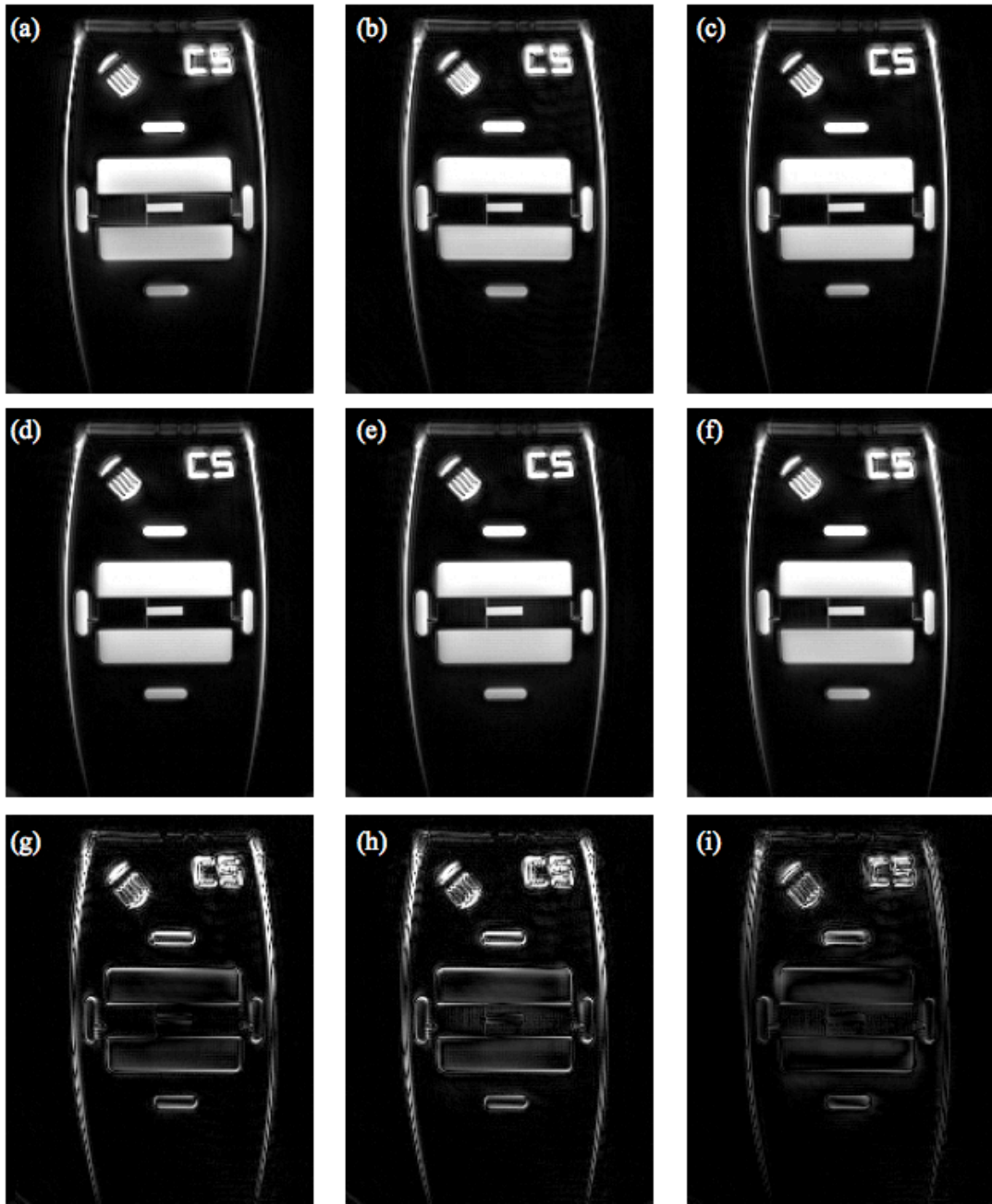
Figure 3.6: Coronal images of acquired phantom data are reconstructed (a) with no correction, (b) with the full k-space trajectory measured using Alley's method, using delays estimated from the (c) first and (d) second iteration of the proposed method, (e) using delays measurements from Alley's method and (f) using constant delays for (X: $+0.75\mu$s, Y: $+2.23\mu$s and Z: $+2.82\mu$s) gradients. The images in (g-i) represent the magnitude of the difference between the respective images in (d-f) and (b), which is assumed to be closest to the truth. The difference images (g-i) are scaled by a factor of 10 compared to the images (a-f), which are windowed the same.

Figure 3.7: Axial images of in-vivo data are reconstructed (a) with no correction, (b) using a second iteration of the proposed variable delay correction. The difference image (c) of (b) and (a) illustrates the differences before and after delay correction. The difference image (c) is scaled by a factor of 10 compared to images (a and b) which are windowed the same.

Chapter 4

DISCUSSION

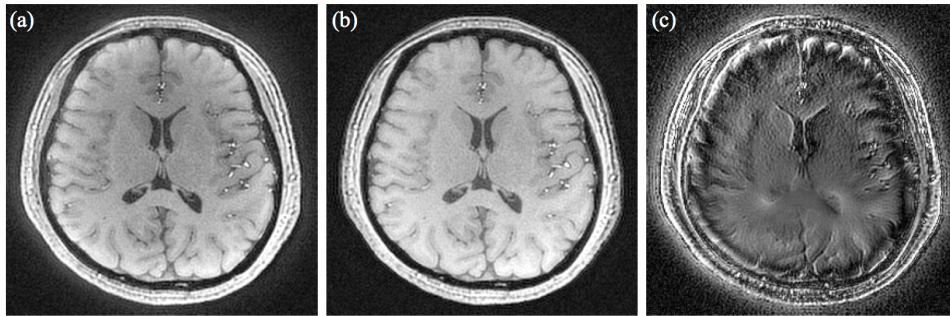The proposed method estimates the delays in the three physical gradients. It was tested using different number of interleaves (16, 48 and 64) keeping the same FOV and resolution on (acquired) phantom data. Figure 3.3a-c for the X, Y and Z gradients respectively shows the delays vary approximately linearly with the gradient angular frequency. Assuming the delays are a function of the gradient angular frequency, the proposed method can be used as a calibration scan for spiral-based trajectories. This assumption may not apply to all MR scanners, as the delays can be system-dependent. Reference [1] determines the system frequency response of two different gradient systems using LTI-based characterization.

The frequency response of the gradients shown in Fig.2.1 of Ref. [1] suggest that time-varying delays can be modeled as the non-linear phase of the LTI transfer function. Given the data for these systems, the delay can be calculated by taking the derivative of the phase with respect to the frequency. This can be used as a method to compare the results of the proposed work. The total acquisition time for the proposed method was 1.7 minutes compared to 4 hours 48 minutes for Alley's method [2]. The slice selection methods are also much faster than Alley's method and can be used as a practical alternative in certain cases.

At present, this method has been tested for axial, sagittal and coronal planes and is yet to be implemented for oblique planes. The method does not account for residual errors from amplitude non-linearity of the gradients. [39] shows the majority of the trajectory error results from system delays, however, some residual error may

still remain from incorrect k-space scaling due to amplitude changes of the gradient waveform [7].

Chapter 5

CONCLUSION

Spiral trajectories are sensitive to the effects of system delays and eddy currents, which can vary over the data-sampling period. These errors can alter the desired sampling locations in k-space, which can result in artifacts in the final reconstructed images. The proposed method was implemented for both synthesized and acquired data, which, when used to correct the trajectory used for reconstruction, resulted in a substantial reduction in these artifacts. The simulation results indicated high accuracy in estimating the applied delays. For acquired data, the implementation of Alley's method [2] further validated the proposed method. The results show the method works well with an assumption of a LSI or similar model for an accurate delay estimate in the initial regions of k-space. Overall, the method is fast, simple and can easily be extended to other spiral based sequences [7].

FUTURE WORK

The work can be extended to other spiral-based trajectories. The method can be further analyzed to estimate errors from gradient non-linearities and concomitant fields. The speed of delay estimation can be increased by futher threading the code to increase the computational efficiency.

REFERENCES

[1] Nii Okai Addy, Holden H Wu, and Dwight G Nishimura. Simple method for MR gradient system characterization and k-space trajectory estimation. Magnetic resonance in medicine : official journal of the Society of Magnetic Resonance in Medicine / Society of Magnetic Resonance in Medicine, 68(1):120–9, July 2012.

[2] M T Alley, G H Glover, and N J Pelc. Gradient characterization using a Fourier-transform technique. Magnetic resonance in medicine : official journal of the Society of Magnetic Resonance in Medicine / Society of Magnetic Resonance in Medicine, 39(4):581–7, April 1998.

[3] Ian C Atkinson, Aiming Lu, and Keith R Thulborn. Characterization and correction of system delays and eddy currents for MR imaging with ultrashort echo-time and time-varying gradients. Magnetic resonance in medicine : official journal of the Society of Magnetic Resonance in Medicine / Society of Magnetic Resonance in Medicine, 62(2):532–7, August 2009.

[4] Prussmann KP Barmet C, Zanche ND. Spatiotemporal magnetic field monitoring for mr. Magn Reson Med, 60:187–197, 2008.

[5] Pauly JM Beatty PJ, Nishimura DG. Rapid gridding reconstruction with a minimal oversampling ratio. IEEE Trans Med Imaging, 24(799-808), 2005.

[6] Marine Beaumont, Laurent Lamalle, Christoph Segebarth, and Emmanuel L Barbier. Improved k-space trajectory measurement with signal shifting. Magnetic resonance in medicine : official journal of the Society of Magnetic Resonance in Medicine / Society of Magnetic Resonance in Medicine, 58(1):200–5, July 2007.

[7] Payal S Bhavsar, Nicholas R Zwart, and James G Pipe. Fast, variable system delay correction for spiral MRI. Magnetic resonance in medicine : official journal of the Society of Magnetic Resonance in Medicine / Society of Magnetic Resonance in Medicine, 00000:1–10, March 2013.

[8] Richard Bitar, General Leung, Richard Perng, Sameh Tadros, Alan R Moody, Josee Sarrazin, Caitlin McGregor, Monique Christakis, Sean Symons, Andrew Nelson, and Timothy P Roberts. MR pulse sequences: what every radiologist wants to know but is afraid to ask. Radiographics : a review publication of the Radiological Society of North America, Inc, 26(2):513–37, 2006.

[9] Kai Tobias Block and Jens Frahm. Spiral imaging: a critical appraisal. Journal of magnetic resonance imaging : JMRI, 21(6):657–68, June 2005.

[10] Ethan K Brodsky, Alexey a Samsonov, and Walter F Block. Characterizing and correcting gradient errors in non-cartesian imaging: Are gradient errors linear time-invariant (LTI)? Magnetic resonance in medicine : official journal of the

Society of Magnetic Resonance in Medicine / Society of Magnetic Resonance in Medicine, 62(6):1466–76, December 2009.

[11] SC Bushong. Magnetic resonance imaging: Physical and biological principles. Mosby, Toronto, 2nd edition., 1996.

[12] J Cheng, B Gagoski, D Bolar, C Triantafyllou, M Hamm, G Krueger, and E Adalsteinsson. Gradient linear system modeling using gradient characterization. In: Proceedings of the 16th Scientific Meeting, International Society for Magnetic Resonance in Medicine, Toronto., page 1155, 2008.

[13] Nigel P Davies and Peter Jezzard. Calibration of gradient propagation delays for accurate two-dimensional radiofrequency pulses. Magnetic resonance in medicine : official journal of the Society of Magnetic Resonance in Medicine / Society of Magnetic Resonance in Medicine, 53(1):231–6, January 2005.

[14] Bénédicte M a Delattre, Robin M Heidemann, Lindsey a Crowe, Jean-Paul Vallée, and Jean-Noël Hyacinthe. Spiral demystified. Magnetic resonance imaging, 28(6):862–81, July 2010.

[15] X Ding, J Tkach, P Ruggieri, J Perl, and T Masaryk. Improvement of spiral MRI with the measured k-space trajectory. Journal of magnetic resonance imaging : JMRI, 7(5):938–40.

[16] J H Duyn, Y Yang, J a Frank, and J W van der Veen. Simple correction method for k-space trajectory deviations in MRI. Journal of magnetic resonance (San Diego, Calif. : 1997), 132(1):150–3, May 1998.

[17] G H Glover. Simple analytic spiral K-space algorithm. Magnetic resonance in medicine : official journal of the Society of Magnetic Resonance in Medicine / Society of Magnetic Resonance in Medicine, 42(2):412–5, August 1999.

[18] Tan H and Meyer CH. Estimation of k-space trajectories in spiral mri. Magn Reson Med, 61:1396–1404, 2009.

[19] R D Hoge, R K Kwan, and G B Pike. Density compensation functions for spiral MRI. Magnetic resonance in medicine : official journal of the Society of Magnetic Resonance in Medicine / Society of Magnetic Resonance in Medicine, 38(1):117–28, July 1997.

[20] P Irarrazabal and D G Nishimura. Fast three dimensional magnetic resonance imaging. Magnetic resonance in medicine : official journal of the Society of Magnetic Resonance in Medicine / Society of Magnetic Resonance in Medicine, 33(5):656–62, May 1995.

[21] John I Jackson, Craig H Meyer, Dwight G Nishimura, and Albert Macovski. Selection of a convolution function for Fourier inversion using gridding (computerised tomography ap - Medical Imaging, IEEE Transactions on. I(3), 1991.

[22] Pipe G. James. Motion correction with propeller mri: Application to head motion and free-breathing cardiac imaging. Magn Reson Med, 42:963–969, 1999.

[23] Kenneth O Johnson. Motion Corrected 3-D MRI Using Spiral Projection Imaging. PhD thesis, Arizona State University, May 2010.

[24] PC. Lauterbur. Image formation by induced local interactions: Examples employing nuclear magnetic resonance. Nature, 242(190-191), 1973.

[25] Andreas E. Lazda. Magnetic resonance data acquisition and image reconstruction using spiral gradients. Masters Thesis. McGill University, Montreal, Canada, 2000.

[26] MH Levitt. Spin Dynamics: Basics of Nuclear Magnetic Resonance. 2nd Edition Chichester, England, 2008.

[27] Allen PS. Liu Q, Hughes DG. Quantitative characterization of the eddy current fields in a 40-cm bore superconducting magnet. Magn Reson Med, 31:73–76, 1994.

[28] GF Mason, T Harshbarger, HP Hetherington, Y Zhang, GM Pohost, and DB Twieg. A method to measure arbitrary k-space trajectories for rapid mr imaging. Magn Reson Med, 61:1396–1404, 2009.

[29] Pierre-jean Nacher. Magnetic Resonance Imaging : From Spin Physics to Medical Diagnosis. pages 1–35, 2008.

[30] DG Nishimura. Principles of Magnetic Resonance Imaging. Department of Electrical Engineering, Stanford University, 1996.

[31] T Onodera, S Matsui, K Sekihara, and H Kohno. A method of measuring field-gradient modulation shapes: Applications to high-speed nmr spectroscopic imaging. J Phys Sci Instrum, 20(416-419), 1987.

[32] NG Papadakis, AA Wilkinson, TA Carpenter, and LD Hall. A general method for measurement of the time integral of variant magnetic field gradients: application to 2d spiral imaging. Magn Reson Imag, 15(567-578), 1997.

[33] Bhavsar S. Payal and Pipe James Grant. Variable gradient delay correction for spiral mri. In: Proceedings of the 19th Annual Meeting ISMRM, Montreal., page 2804, 2011.

[34] Dana C Peters, J Andrew Derbyshire, and Elliot R McVeigh. Centering the projection reconstruction trajectory: reducing gradient delay errors. Magnetic resonance in medicine : official journal of the Society of Magnetic Resonance in Medicine / Society of Magnetic Resonance in Medicine, 50(1):1–6, July 2003.

[35] James G Pipe, Nicholas R Zwart, Eric a Aboussouan, Ryan K Robison, Ajit Devaraj, and Kenneth O Johnson. A new design and rationale for 3D orthogonally oversampled k-space trajectories. Magnetic resonance in medicine : official journal of the Society of Magnetic Resonance in Medicine / Society of Magnetic Resonance in Medicine, 66(5):1303–11, November 2011.

[36] JG Pipe and P Menon. Sampling density compensation in mri: Rationale and an iterative numerical solution. Magnetic Resonance in Medicine, 41(179-186), 1999.

[37] V Rasche, R Proksa, R Sinkus, P Bornert, and Eggers H. Resampling of data between arbitrary grids using convolution interpolation. IEEE Transactions on Medical Imaging, 18(385-392), 1999.

[38] John P Ridgway. Cardiovascular magnetic resonance physics for clinicians: part I. Journal of cardiovascular magnetic resonance : official journal of the Society for Cardiovascular Magnetic Resonance, 12(1):71, January 2010.

[39] Ryan K Robison, Ajit Devaraj, and James G Pipe. Fast, simple gradient delay estimation for spiral MRI. Magnetic resonance in medicine : official journal of the Society of Magnetic Resonance in Medicine / Society of Magnetic Resonance in Medicine, 63(6):1683–90, June 2010.

[40] Christopher Joseph Wargo. High Resolution MRI of the human brain using reduced-FOV techniques at 7 Tesla. PhD thesis, Vanderbilt University, 2011.

[41] HP Zhang Y Hetherington, EM Stokely, GF Mason, and DB. Twieg. A novel k-space trajectory measurement technique. Magn Reson Med, 39:999–1004, 1998.

[42] Nicholas R Zwart, Kenneth O Johnson, and James G Pipe. Efficient sample density estimation by combining gridding and an optimized kernel. Magnetic resonance in medicine : official journal of the Society of Magnetic Resonance in Medicine / Society of Magnetic Resonance in Medicine, 67(3):701–10, March 2012.